J. Fluid Mech. (2006), vol. 548, pp. 113–131. © 2006 Cambridge University Press
doi:10.1017/S0022112005007470 Printed in the United Kingdom

Generation of micro gas bubbles of uniform diameter in an ultrasonic field

By TOSHINORI MAKUTA[1,2], FUMIO TAKEMURA[2], EIJI HIHARA[1], YOICHIRO MATSUMOTO[3] AND MASAHIRO SHOJI[2,3]

[1]Graduate School of Frontier Sciences, The University of Tokyo, 7-3-1 Hongo, Bunkyo-ku, Tokyo, 113-8656, Japan

[2]National Institute of Advanced Industrial Science and Technology, 1-2-1 Namiki, Tsukuba, Ibaraki, 305-8564, Japan

[3]Department of Mechanical Engineering, The University of Tokyo, 7-3-1 Hongo, Bunkyo-ku, Tokyo, 113-8656, Japan

(Received 14 March 2005 and in revised form 20 July 2005)

Consecutive images of the fragmentation of capillary waves in an ultrasonic field were obtained using a high-speed video camera through a microscope at a frame rate of 500 000 frames per second. The images showed that micro bubbles of uniform diameter from 4 to 15 μm were generated at a constant periodic rate when a small amount of gas was introduced (via a needle) into a highly viscous liquid whose kinematic viscosity was between 5 and 100 mm^2 s^{-1}. Conditions for stable generation of micro bubbles of uniform diameter were also studied by changing the inner diameter of the needle between 0.08 and 0.34 mm, excitation frequency of around 18.77 and 42.15 kHz, kinematic viscosity of liquid between 5 and 100 mm^2 s^{-1}, surface tension between 20 and 34 mN m^{-1}, and viscosity of gas between 9.0 and 31.7 μPa s. Results revealed that (i) a projection is formed on the oscillatory gas–liquid interface and micro bubbles are released from the tip of the projection; (ii) gas viscosity critically affects the formation of the projection and should be around 20.0 μPa s for stable mother bubble oscillation; (iii) conditions for stable generation of micro bubbles are also affected by excitation frequency, surface tension and viscosity of the liquid, and dimensions of the needle; (iv) two controlling parameters for stable generation are the Weber number ($We = \rho f^2 d_{in}^3/\sigma$, where ρ is the density of the liquid, f is the excitation frequency, d_{in} is the inner diameter of the needle, and σ is the surface tension) and the Womersley number ($Wo = d_{in}(f/\nu)^{1/2}$, where ν is the kinematic viscosity of liquid); and (v) uniform-diameter micro bubbles are generated stably when $We < 300$ and $2 < Wo < 5$. Under the conditions where micro bubbles of uniform diameter were stably generated, the bubble diameter increased almost linearly with increasing gas pressure inside the needle. The gradient of this linear function can be expressed as a function of Wo, We, and the normalized outer diameter of the needle, and decreases either with decreasing inner diameter of the needle or with increasing excitation frequency, surface tension and viscosity of the liquid, and outer diameter of the needle.

1. Introduction

The mechanism for ultrasonic atomization of liquid droplets is generally explained by the *cavitation hypothesis* or the *capillary hypothesis*. In the cavitation hypothesis, atomization occurs owing to the shock wave generated by the collapse of bubbles

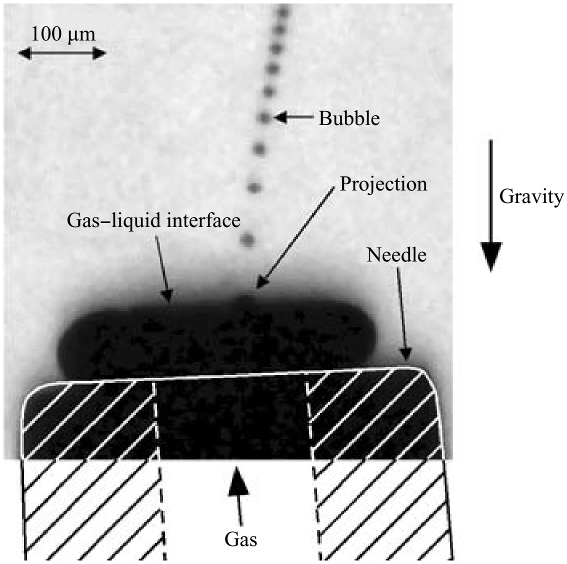

FIGURE 1. Typical photograph showing micro bubbles of uniform diameter.

near a free surface. In the capillary wave hypothesis, atomization occurs owing to fragmentation of the capillary wave induced in an ultrasonic field. The cavitation hypothesis is often applied in the high-frequency regime (>100 kHz), whereas the capillary hypothesis is applied in the lower-frequency regime (<100 kHz; see, for example, Kirpalani & Toll 2002). The capillary wavelength in an ultrasonic field can be obtained from the well-known Kelvin equation (Rayleigh 1945) describing the relation between a capillary wavelength and a capillary wave frequency as $\lambda^3 = 2\pi\sigma/(\rho f_k^2)$. Here, λ is the capillary wavelength, ρ is the density of the liquid, f_k is a capillary wave frequency, and σ is the surface tension. Although f_k is defined as $nf/2$ (f is excitation frequency, $n = 1, 2, 3, \ldots$), it is improbable that ranges other than $n = 1$ have to be considered for capillary waves on plane surfaces (Eisenmenger 1959). Lang (1962) determined experimentally a strong correlation between the median size of droplets D atomized by ultrasonic waves and the theoretically estimated capillary wavelength; this correlation is expressed as $D = 0.34\,(8\pi\sigma/(\rho f^2))^{1/3} = 0.34\,\lambda$. The fragmentation mechanism of bubbles in an ultrasonic field can also apparently be explained by the capillary hypothesis. For instance, Walmsley, Laird & Williams (1985) measured the size distribution of bubbles fragmentized by an ultrasonic wave, and showed that the average size of the bubbles is about 30 % of the theoretical capillary wavelength. Because the measured sizes of bubbles vary and bubbles much smaller than $D = 0.34\,\lambda$ are produced, however, the fragmentation mechanism of the capillary wave is not yet sufficiently understood.

The purpose of this study was to clarify the mechanism of the generation process of micro bubbles in an ultrasonic field. Consecutive images of the fragmentation of capillary waves in an ultrasonic field were obtained by using a high-speed video camera through a microscope at a frame rate of 500 000 frames per second. The images showed that micro bubbles of uniform diameter from 4 to 15 μm were generated at constant rate when a small amount of gas was introduced (via a needle) into a highly viscous liquid whose kinematic viscosity is between 5 and 100 $mm^2\,s^{-1}$. Figure 1 shows a typical photograph of micro bubbles of uniform diameter. Because the bubbles

	1	2	3	4	5	6	7	8
d_{in} (mm)	0.08	0.11	0.13	0.13	0.18	0.21	0.26	0.34
d_{out} (mm)	0.20	0.24	0.26	0.47	0.36	0.41	0.46	0.64

TABLE 1. Inner and outer diameters of needles.

are uniform, this generation process can be used to help clarify the fragmentation mechanism of bubbles in an ultrasonic field. By changing the conditions, including excitation frequency, inner and outer diameters of the needle, surface tension and viscosity of the liquid, viscosity of the gas, pressure amplitude in the ultrasonic field, and gas pressure inside the needle, we produced micro bubbles of uniform diameter and investigated how these parameters hydrodynamically affect the generation process as a function of Weber number ($We = \rho f^2 d_{in}^3/\sigma$ where d_{in} is the inner diameter of the needle) and Womersley number ($Wo = d_{in}(f/\nu)^{1/2}$ where ν is the kinematic viscosity of liquid). Results revealed that (*a*) a projection is formed on the oscillatory gas–liquid interface and micro bubbles are released from the tip of the projection; (*b*) gas viscosity critically affects both the formation of a projection and the stable oscillation of the mother bubble; (*c*) micro bubbles of uniform diameter from 4 to 15 μm smaller than $0.34\,\lambda$ are produced and that the diameter is not proportional to the capillary wavelength. Results also showed that the diameter of the micro bubbles can be almost linearly controlled by adjusting the gas pressure inside the needle, and that the gradient of this linear function expressing the bubble diameter is affected by the excitation frequency, inner and outer diameters of the needle, and surface tension and viscosity of the liquid.

2. Experimental set-up and procedure

Figure 2 shows a schematic of the experimental set-up used to generate and observe the generation process of micro bubbles. The set-up consisted of a test section, ultrasonic wave generator, needle-type hydrophone, needle, microscope, CCD camera, PC and a light source. The test section was a 100 mm long acrylic channel with a 400 mm × 56 mm cross-section. The needle was inserted from the bottom of the channel and gas was introduced through the needle. Eight types of stainless steel needles with blunt needle point style (Hamilton, series of Point Style 3) of different inner and outer diameters (d_{in} and d_{out}, respectively) were tested, as summarized in table 1. Because each surface of a needle tip has minute roughness, the gas–liquid interface does not always oscillate symmetrically about the gravity axis and the produced bubbles do not always ascend vertically to the surface of the needle tip as shown in figure 1. Two plates were set vertically in the test section and a ferrite magnetostrictive ultrasonic transducer (TDK, V2X) was fixed to one side of the plate (Detail A in figure 2). By adjusting the distance between the two plates, a standing wave was formed between the two plates. The ultrasonic transducer was connected to an amplifier (Mess-Tek, M2617) and f was input through a function generator (Toyo, 2416A). Two ultrasonic transducers of different f, 18.77 kHz and 42.15 kHz, were used. The sound pressure was measured using the hydrophone (Imotec, Type80-0.5-4.0), which can detect pressure changes up to 10 MHz.

Two different types of silicone oil were used as the carrier liquid: dimethyl siloxane polymer (KF-96, Shinetsu) with kinematic viscosity $\nu = 5$, 10, 20, 30, 50 or 100 mm^2 s^{-1}, and methylphenyl siloxane polymer (HIVAC, Shinetsu) with $\nu = 37$ or 160 mm^2 s^{-1}.

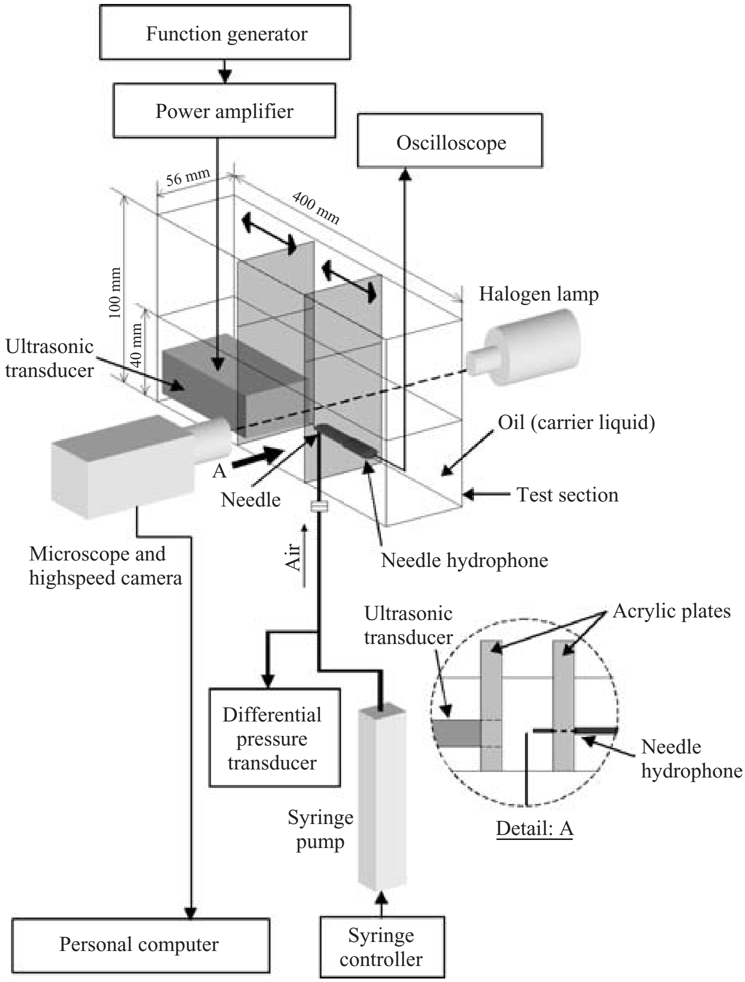

FIGURE 2. Schematic of experimental set-up to generate and observe the generation of micro gas bubbles of uniform diameter.

ν ($mm^2\,s^{-1}$)	5	10	20	30	50	100
σ ($mN\,m^{-1}$)	19.7	20.1	20.8	20.8	20.8	20.9

TABLE 2. Properties of KF-96 silicone oil.

ν ($mm^2\,s^{-1}$)	37	160
σ ($mN\,m^{-1}$)	33.9	34.3

TABLE 3. Properties of HIVAC silicone oil.

The properties of KF-96 and HIVAC at 25 °C are shown in tables 2 and 3, respectively. The HIVAC was used to study the effect of the surface tension (σ) on the micro bubble generation. We mixed two different HIVAC with $\nu = 37$ and $160\,mm^2\,s^{-1}$ and produced a mixed HIVAC with $\nu = 50\,mm^2\,s^{-1}$, where ν was measured using a

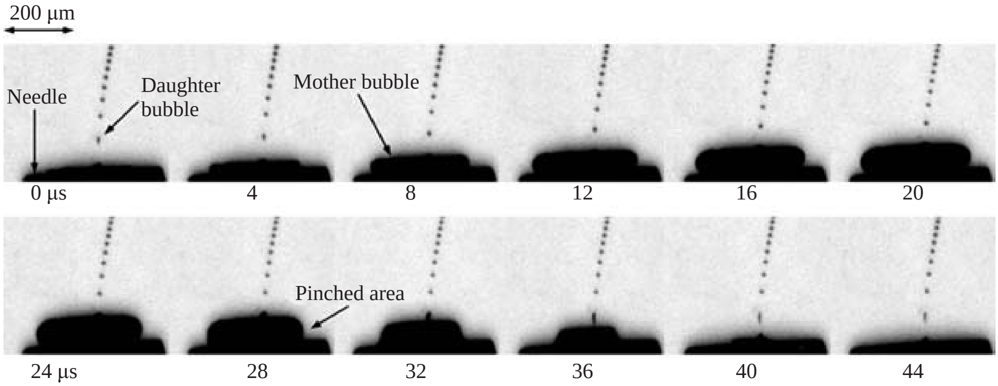

FIGURE 3. Consecutive images showing stable periodic capillary wave and micro bubbles of uniform diameter.

rotating viscometer with double cylinders (Tokimec, DVL-B II). The surface tensions of the silicone oils were measured by Shinetsu.

All experiments were done at room temperature and atmospheric pressure. The test section was filled with the oil, and air was introduced at a flow rate of about $2\,\mu l\,min^{-1}$ through the needle. By adjusting the distance between the two plates, a standing wave was formed between the two plates. By regulating the output current from the amplifier, the pressure amplitude of the standing wave was adjusted to around 10 kPa. Because the tip of the needle-type hydrophone was 1.2 mm in diameter, it did not disturb the sound field. Images of the oscillatory gas–liquid interface and the bubbles released from this interface by ultrasound were taken through a microscope by a high-speed camera (Shimadzu, PCV-2) with a resolution of 312×260 pixels at 500 000 frames per second and a halogen lamp as a light source (Moritex, MHF-G150LR). The diameter of the bubbles was precisely measured in the images based on 1 pixel in the image corresponding to 2.8 μm.

3. Result and discussion

3.1. *Generation of micro bubbles of uniform diameter*

Figure 3 shows typical consecutive images of a stable periodic capillary wave and of single bubbles of uniform diameter (about 12 μm) generated at each oscillation (about every 50 μs) with $f = 18.77$ kHz and pressure amplitude (P_{amp}) of about 10.3 kPa. KF-96 Silicone oil with $\nu = 50\,mm^2\,s^{-1}$ and $\sigma = 20.8\,mN\,m^{-1}$ was used as the carrier liquid, $d_{in} = 0.26$ mm, and the airflow rate was about $2\,\mu l\,min^{-1}$. The flat surface is the tip of the needle, the bubble oscillating on the tip is the 'mother' bubble, and the bubbles flowing upward are the 'daughter' bubbles released from the mother bubble. For simplicity, here we will refer to the gas–liquid interface at the mother bubble as 'the interface'.

Figure 3 shows that the interface oscillated while maintaining a relatively axially symmetric surface. From 0 to 24 μs, the mother bubble expanded toward the carrier liquid. From 24 to 36 μs, the interface started to shrink and a 'pinched area' was formed. From 36 to 44 μs, the pinched area reached the centre of the mother bubble and an elongated small bubble was released from the interface. From 44 to 52 μs, the interface retracted into the needle and returned to its initial stage. The mother bubble oscillates once per forcing cycle, and a micro bubble is formed once per forcing cycle.

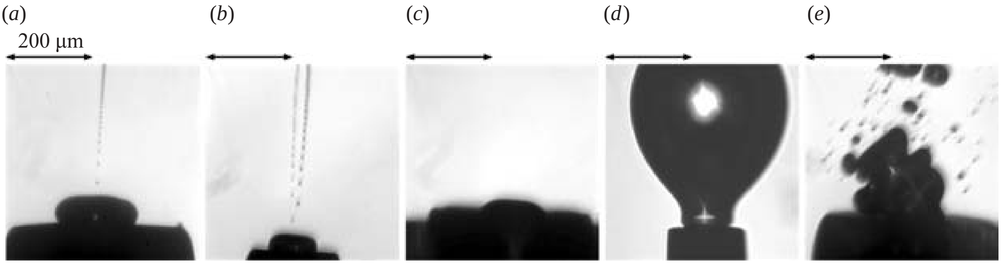

FIGURE 4. Photographs showing typical generation states of bubbles ($f = 18.77$ kHz). (*a*) State I. $d_{in} = 0.13$ mm, $d_{out} = 0.47$ mm, $\nu = 20\,\mathrm{mm^2\,s^{-1}}$, $\sigma = 21\,\mathrm{mN\,m^{-1}}$. (*b*) State II. $d_{in} = 0.11$ mm, $d_{out} = 0.24$ mm, $\nu = 5\,\mathrm{mm^2\,s^{-1}}$, $\sigma = 21\,\mathrm{mN\,m^{-1}}$. (*c*) State III. $d_{in} = 0.34$ mm, $d_{out} = 0.64$ mm, $\nu = 50\,\mathrm{mm^2\,s^{-1}}$, $\sigma = 21\,\mathrm{mN\,m^{-1}}$. (*d*) State IV. $d_{in} = 0.08$ mm, $d_{out} = 0.20$ mm, $\nu = 30\,\mathrm{mm^2\,s^{-1}}$, $\sigma = 21\,\mathrm{mN\,m^{-1}}$. (*e*) State V. $d_{in} = 0.13$ mm, $d_{out} = 0.47$ mm, $\nu = 5\,\mathrm{mm^2\,s^{-1}}$, $\sigma = 20\,\mathrm{mN\,m^{-1}}$.

The stable oscillations and the stable generation of micro bubbles of uniform diameter indicated in figure 3 were observed when $\nu = 5$ to $100\,\mathrm{mm^2\,s^{-1}}$ as shown later. On the other hand, when $d_{in} = 0.13$ mm, $d_{out} = 0.47$ mm, $\nu = 5\,\mathrm{mm^2\,s^{-1}}$, and $\sigma = 20\,\mathrm{m\,Nm^{-1}}$, bubbles of various sizes were released from the interface (figure 4*e*). When $d_{in} = 0.34$ mm, $d_{out} = 0.64$ mm, $\nu = 50\,\mathrm{mm^2\,s^{-1}}$, and $\sigma = 21\,\mathrm{mN\,m^{-1}}$, no bubbles were released from the interface (figure 4*c*). The viscous effect stabilizes the oscillation of the gas–liquid interface at the tip of the needle (Prosperetti 1977; Hao & Prosperetti 1999) and is one of the parameters that controls the generation of micro bubbles of uniform diameter. In this study, we investigated the conditions for micro bubble generation of uniform diameter by changing various parameters, including f, P_{amp}, d_{in}, d_{out}, P_g and ν and σ of the carrier liquid (silicone oil). The magnitude of the gas viscosity, μ_g, is particularly important for micro bubble generation as shown later.

First, we define the following four states for expressing the states of bubble generation.

State I. State where micro bubbles of uniform diameter are generated stably at a periodic rate (figure 4*a*). The regime of this state depends on parameters such as f, P_{amp}, d_{in}, d_{out}, P_g, μ_g, ν and σ.

State II. State where micro bubbles of uniform diameter are generated irregularly or several micro bubbles of uniform diameter are generated (figure 4*b*). This state is the transition from State I to State IV.

State III. State where no micro bubbles are generated (figure 4*c*), because energy supplied to the mother bubble is not sufficient to distort the mother bubble.

State IV. State where a large single bubble is generated when P_{amp} is small and P_g is high (figure 4*d*). When P_{amp} increases, the large bubble is distorted and further generates bubbles of various sizes (figure 4*e*).

Note that even though micro bubbles of uniform diameter are generated stably, the shape of the interface depends on the experimental conditions, including f, P_{amp}, d_{in}, d_{out}, P_g, μ_g and ν and σ of the carrier liquid. Figure 5 shows consecutive images of the oscillation of the mother bubble at the tip of the needle for about 1 period. As shown in figure 5(*a*), a surface wave was generated at the edge of the tip of the needle and propagated toward the centre of the needle. The wave formed the projection shown in the image at 48 μs and bubbles were generated by the detachment of the projection from the surface. After the detachment, the projection disappeared and did not form again until the next surface wave reached the centre. In contrast, as shown in figure 5(*b*), the surface of the mother bubble formed into a step as shown in the image

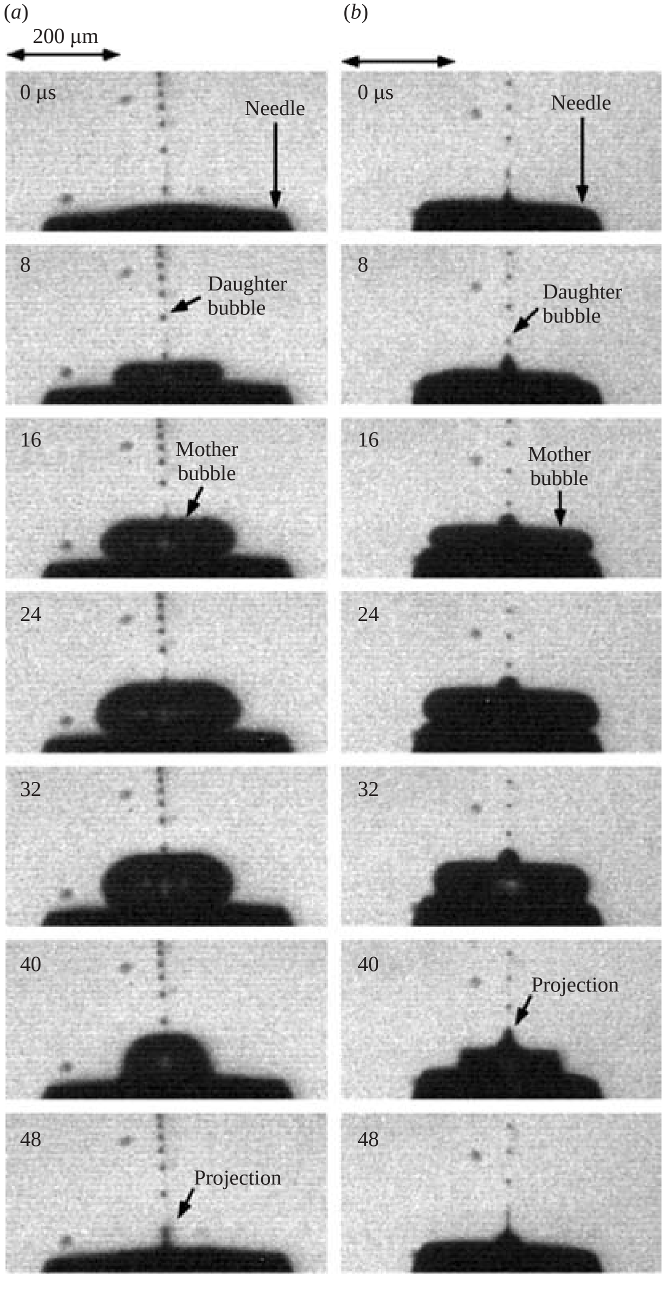

FIGURE 5. Consecutive images showing generation of micro-bubbles ($f = 18.77$ kHz). (*a*) $P_{amp} = 7.5$ kPa, $d_{in} = 0.13$ mm, $d_{out} = 0.47$ mm, $\nu = 20\,\mathrm{mm^2\,s^{-1}}$, $\sigma = 21\,\mathrm{mN\,m^{-1}}$. (*b*) $P_{amp} = 11.7$ kPa, $d_{in} = 0.18$ mm, $d_{out} = 0.36$ mm, $\nu = 50\,\mathrm{mm^2\,s^{-1}}$, $\sigma = 21\,\mathrm{mN\,m^{-1}}$.

at 40 μs. Bubbles were generated from the projection, and the projection formed again just after the detachment of the micro bubbles.

Because micro bubbles are released from the tip of the projection for both cases, the projection is crucial for micro bubble generation. Although the mechanism for the formation of the projection is not completely clear, one possible explanation is as

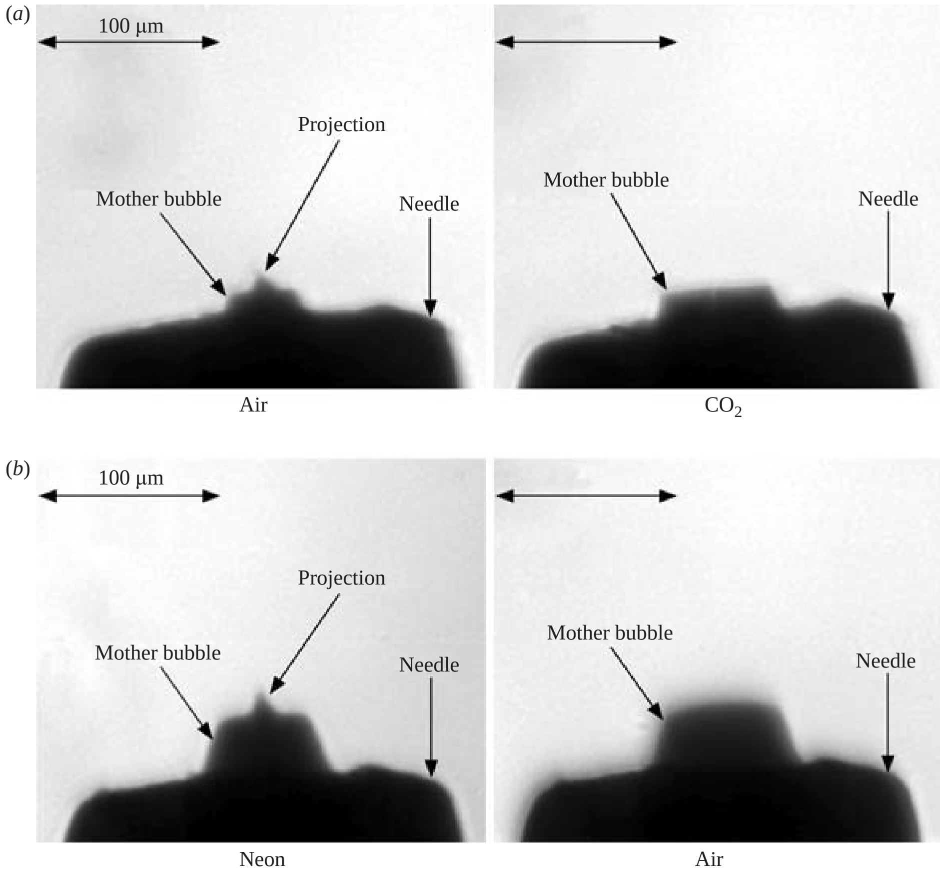

FIGURE 6. Instantaneous images of the gas–liquid interface of a mother bubble. (*a*) $P_{amp} = 6.3\,\text{kPa}$, $P_g = 4.0\,\text{kPa}$, $d_{in} = 0.11\,\text{mm}$, $d_{out} = 0.24\,\text{mm}$, $\nu = 30\,\text{mm}^2\,\text{s}^{-1}$, $\sigma = 21\,\text{mN}\,\text{m}^{-1}$, (*b*) $P_{amp} = 9.1\,\text{kPa}$, $P_g = 5.0\,\text{kPa}$, $d_{in} = 0.11\,\text{mm}$, $d_{out} = 0.24\,\text{mm}$, $\nu = 30\,\text{mm}^2\,\text{s}^{-1}$, $\sigma = 21\,\text{mN}\,\text{m}^{-1}$.

follows. When a liquid jet impinges vertically onto a free surface, a circular singularity forms at the crossing line of the distorted free surface and the liquid jet. The gas entrained by the liquid jet flows into a narrow space near the singularity and increases the pressure near the singularity. This pressure is known as lubrication pressure, and pushes out the free surface near the singularity (Eggers 2001). Using numerical simulation, Eggers (2001) showed the importance of gas viscosity for lubrication pressure. Although his calculation neglected fluid inertia, gas viscosity might also be crucial for the formation of the projection in our experiments because the same projection with the cusp appeared in his numerical simulations. In our study, the effects of gas viscosities were investigated by using hydrogen, carbon dioxide, air and neon, whose viscosities are 9.0, 14.9, 18.6 and 31.7 µPa s, respectively. Figure 6 shows the instantaneous images of the gas–liquid interface of the mother bubble for air and carbon dioxide gas (figure 6*a*) and for neon gas and air (figure 6*b*) under the same experimental conditions. The figure shows that the gas viscosity affected the shape of the interface even though the experimental conditions were the same and that the projection appeared with increasing gas viscosity. These results coincide with the prediction by Eggers (2001). Our experimental results show the difficulty in stably producing micro bubbles of low viscosity gases, including hydrogen and carbon dioxide gases, because of the difficulty in stable formation of the projection. In contrast, although neon gas is viscous enough to induce a projection, the instability of the oscillation of the mother bubble increased because the induced projection was too large. In conclusion, stable micro bubble generation is critically affected by gas viscosity and is limited to around 20.0 μPa s. Therefore, only air was used in the following analysis.

3.2. *Conditions for stable generation of micro bubbles of uniform diameter*

As shown by figures 5 and 6, the generation process of micro bubbles is complicated, and the shape of the surface wave and the detachment mechanism of the micro bubbles are too difficult to analyse precisely. Therefore, in this study, we investigated only the conditions for stable generation of micro bubbles of uniform diameter. Table 4 shows the experimental results of the generation states categorized as States I and II as a function of P_{amp} for KF-96 at $f = 18.77$ kHz, for KF-96 at $f = 42.15$ kHz, and for HIVAC with $\nu = 50\,\mathrm{mm^2\,s^{-1}}$ at $f = 18.77$ kHz. Table 4(*a*) shows that State I, i.e. the regime where micro bubbles are stably generated, occurred when d_{in} was small and ν was low, or when d_{in} was large and ν was high. When ν was increased, the necessary P_{amp} increased. Although the relationship between d_{in} and P_{amp} is weak for the conditions of State I, P_{amp} roughly decreased as d_{in} increased. When $f = 42.15$ kHz (table 4*b*), the conditions for stable generation shifted to smaller d_{in}, because the increase in f caused the wavelength of the surface wave to decrease. P_{amp} for stable generation increased according to the increase in f. For HIVAC (table 4*c*), d_{in} for stable generation was limited to between 0.11 and 0.21 mm, indicating that an increase in σ decreased the regime of stable generation. Because P_{amp} for stable generation increased with σ, regulating P_{amp} becomes difficult owing to the narrow range of P_{amp} for stable generation.

Including the surface tension term, the Navier–Stokes equation can be expressed as follows (see Brackbill, Kothe & Zemach 1992).

$$\frac{\partial \boldsymbol{u}}{\partial t} + (\boldsymbol{u}\cdot\nabla)\boldsymbol{u} = -\frac{1}{\rho}\nabla p + \nu\Delta\boldsymbol{u} + \sigma\kappa\delta(\varphi)\boldsymbol{n}, \tag{1}$$

where $\boldsymbol{u}$ is the velocity vector, κ is the curvature of the interface, $\boldsymbol{n}$ denotes the normal unit vector to the interface, and $\delta(\varphi)$ is a delta function of the normal distance φ to the bubble interface with the origin at the interface. All physical quantities can be made dimensionless:

$$t^* = ft, \quad \boldsymbol{u}^* = \frac{1}{f d_{in}}\boldsymbol{u}, \quad p^* = \frac{p}{\rho f^2 d_{in}^2}, \quad \kappa^* = d_{in}\kappa. \tag{2}$$

Introducing the dimensionless parameters $Wo = d_{in}\sqrt{f/\nu}$ and $We = \rho f^2 d_{in}^3/\sigma$, the Navier–Stokes equation becomes

$$\frac{\partial \boldsymbol{u}^*}{\partial t^*} + (\boldsymbol{u}^*\cdot\nabla)\boldsymbol{u}^* = -\nabla p^* + \frac{1}{Wo^2}\Delta\boldsymbol{u}^* + \frac{1}{We}\kappa^*\delta(\varphi)\boldsymbol{n}, \tag{3}$$

where the Womersley number (Wo) denotes the ratio of pulsatile to viscous forces and the Weber number (We) denotes the ratio of inertial and surface tension forces. Wo is the dimensionless number often used in studying oscillatory fields; for example, Staatman *et al.* (2002) investigated the stability of plain pulsatile Poiseuille flow as a function of Wo.

(*a*)

		d_{in} (mm)						
		0.08	0.11	0.13	0.18	0.21	0.26	0.34
P_{amp} (kPa) State		0.20	0.24	0.47	0.36	0.41	0.46	0.64
		d_{out} (mm)						
ν (mm^2 s^{-1})	5	2.3	2.1	–	–	–	–	–
		I	II					
	10	4.0	2.3	5.8	–	–	–	–
		I	I	II				
	20	7.4	8.9	7.5	7.5	12.9	6.9	–
		I	I	I	I	I	II	–
	30	9.4	9.9	12.3	13.6	11.6	19.5	–
		I	I	I	I	I	II	–
	50	14.8	14.5	13.0	11.7	15.0	12.6	–
		I	I	I	I	I	I	–
	100	27.6	32.7	24.5	18.9	21.1	21.6	21.8
		II	II	II	I	I	I	II

(*b*)

		d_{in} (mm)						
		0.08	0.11	0.13	0.18	0.21	0.26	0.34
P_{amp} (kPa) State		0.20	0.24	0.47	0.36	0.41	0.46	0.64
		d_{out} (mm)						
ν (mm^2 s^{-1})	5	–	–	–	–	–	–	–
	10	5.0	16.3	–	–	–	–	–
		I	II					
	20	9.6	8.7	–	–	–	–	–
		I	I					
	30	11.6	11.8	–	–	–	–	–
		I	I					
	50	21.6	15.8	18.2	–	–	–	–
		I	I	I				
	100	–	41.9	–	–	–	–	–
			II					

(*c*)

	d_{in} (mm)						
	0.08	0.11	0.13	0.18	0.21	0.26	0.34
P_{amp} (kPa) State	0.20	0.24	0.47	0.36	0.41	0.46	0.64
	d_{out} (mm)						
	25	18.1	17.3	19.2	17.5	21.2	
	II	I	I	I	I	II	–

Table 4. Experimental results of uniform-diameter micro bubble generation (*a*) in KF-96 silicone oil at $f = 18.77$ kHz; (*b*) in KF-96 silicone oil at $f = 42.15$ kHz; (*c*) in HIVAC silicone oil with $\nu = 50\,\text{mm}^2\,\text{s}^{-1}$ at $f = 18.77$ kHz.

Figure 7 shows the experimental data in table 4 plotted on $Wo - We$ plots. Based on figure 7, micro bubbles of uniform diameter were stably generated at $We < 300$ and $2 < Wo < 5$. When $Wo > 5$, the patterns of the oscillation were not periodic, as shown in figure 4(*e*), and many bubbles of various sizes were released from the interface at

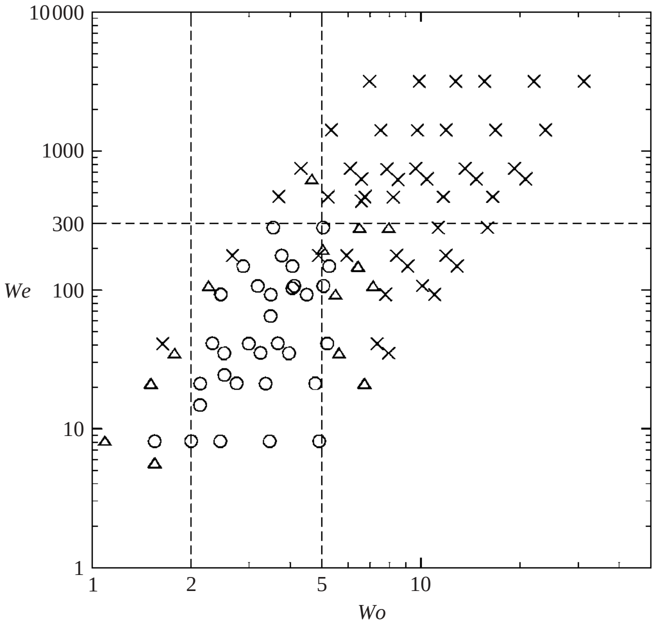

FIGURE 7. State diagram of bubble generation (*We*–*Wo* plot). ○, State I; △, State II; ×, States III or IV.

each oscillation, because for this *Wo* the inertial effect dominates the viscous effect. We saw a similar pattern for water ($Wo = 11.0$ for $d_{in} =$ 0.08 mm and $f = 18.77$ kHz; data not shown), suggesting that it is difficult to generate bubbles of uniform diameter in water because to satisfy $Wo < 5.0$, d_{in} should be reduced by half ($d_{in} = 0.04$ mm) or f should be reduced to quarter ($f = 4.7$ kHz) of that used in our experiments. When $We > 300$, the inertial effect dominates the surface tension effect and reduces the recovery force of the shape of the interface. Consequently, many bubbles with various sizes were released from the interface at each oscillation, as observed when $Wo > 5$. When $Wo < 2$, the shape of the interface was not distorted sufficiently to release bubbles owing to strong viscous effect, as shown in figure 4(*c*).

Even when $2 < Wo < 5$, the oscillation became stable without strong distortion of the interface, and no bubbles were generated owing to strong surface tension effect for small *We*. The minimum *We* for the stable generation of micro bubbles of uniform diameter could not be determined because we could not obtain data for $We < 8.16$ in the regime of $2 < Wo < 5$.

To generate micro bubbles of uniform diameter, P_{amp} of the ultrasonic field is critical and must be carefully controlled. The critical P_{amp} depends on several parameters, including f, d_{in}, d_{out}, ν, σ and the depth of the liquid in the test section. Here, we investigated the critical P_{amp} of the ultrasonic field. Note that the measured P_{amp} deviated from the real P_{amp} because the pressure was measured 2 mm from the needle to avoid disturbing the oscillation of the mother bubble. Because the wavelength of the ultrasound was 25 mm even for $f = 40$ kHz, and thus sufficiently long compared with the 2 mm distance, the deviation was small. Figure 8 shows a typical diagram of the generation state of the micro bubbles for various P_{amp} and P_g, and for $f = 18.77$ kHz, $\nu = 30\,\mathrm{mm^2\,s^{-1}}$, $\sigma = 21\,\mathrm{mN\,m^{-1}}$, $d_{in} = 0.11$ mm, and $d_{out} = 0.24$ mm. The experimental results show that the State I regime is narrow and that the maximum variation in both P_{amp} and P_g for State I is 5 kPa. State I became large with decreasing σ when

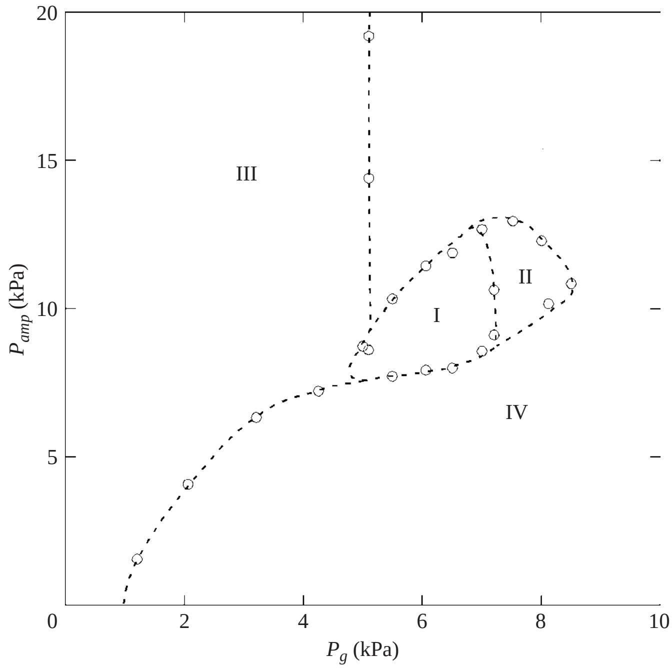

FIGURE 8. State diagram of bubble generation (P_{amp}–P_g plot). ○, experimental data ($f = 18.77$ kHz, $d_{in} = 0.11$ mm, $d_{out} = 0.24$ mm, $\nu = 30\,\mathrm{mm^2\,s^{-1}}$, $\sigma = 21\,\mathrm{mN\,m^{-1}}$).

$\sigma > 20$ and was dependent on σ, d_{in}, P_g and f. For instance, when $f = 18.77$ kHz and $d_{in} = 0.08$ mm, the State I regime at $\nu = 30\,\mathrm{mm^2\,s^{-1}}$ was wider than that at $\nu = 50\,\mathrm{mm^2\,s^{-1}}$. However, when $f = 42.15$ kHz, $d_{in} = 0.11$ mm, the State I regime at $\nu = 30\,\mathrm{mm^2\,s^{-1}}$ was narrower than that at $\nu = 50\,\mathrm{mm^2\,s^{-1}}$. The State I regime was relatively large when $Wo = 2.0 \sim 3.5$ and narrow when $Wo = 3.5 \sim 5.0$. However, even when $Wo = 2.0 \sim 3.5$, the critical P_{amp} became high for a liquid with high ν or for high f, because the flow field around the needle became turbulent and micro bubbles of uniform diameter were therefore not generated. When the depth of a liquid is changed, the critical P_{amp} increases owing to increasing static liquid pressure. The depth, however, has little affect on P_g.

State II is the transition from State I to State IV, and 'contacts' State I at the point where both P_{amp} and P_g are high. State III is observed when the gas pressure is low, and no bubbles are generated (figure 4*c*). State IV is observed when P_g is high. Also in State IV, a large bubble is generated when P_{amp} is small (figure 4*d*). When P_{amp} increases, the mother bubble is distorted and further generates bubbles of various sizes (figure 4*e*).

3.3. *Dependency of parameters on the diameter of micro bubbles*

The experimental results revealed that daughter bubble diameter d_b can be controlled by changing P_g in State I. Although P_{amp} also affects the bubble diameter, here we investigated only the effect of P_g on d_b because controlling P_{amp} is more difficult than controlling P_g. Table 5 summarizes the experimental conditions used to investigate this effect. Figures 9 and 10 show the instantaneous images of the evolution of the generated micro bubbles for increasing P_g for Exps 1, 2, 6 and 7. Figure 9 shows the

Exp.	f (kHz)	P_{amp} (kPa)	d_{in} (mm)	ν (mm^2 s^{-1})	σ (mN m^{-1})	Wo	We	d^*_{out}
1	18.77	8.7	0.11	30	21	2.75	21.2	2.2
2	42.15	24.8	0.11	50	21	3.19	107.0	2.2
3	18.77	10.1	0.08	30	21	2.00	8.2	2.5
4	18.77	13.0	0.13	30	21	3.25	35.0	2.0
5	18.77	10.5	0.13	30	21	3.25	35.0	3.6
6	18.77	8.5	0.18	30	21	4.50	93.0	2.0
7	18.77	13.9	0.11	50	21	2.13	21.2	2.2
8	18.77	23.4	0.11	75	34	1.74	14.8	2.2

TABLE 5. Experimental conditions for measuring daughter bubble diameter d_b.

images when the volume of the mother bubble was at its maximum, and figure 10 shows those immediately after the daughter bubbles had detached from the mother bubble.

The results of Exp. 1 show that d_b increased with increasing P_g. Exp. 2 also showed this tendency, although the shape of the mother bubble differed from that in Exp. 1. For both cases, the maximum volume of the mother bubble increased with increasing P_g and the detachment point of the daughter bubbles shifted upward. These results reveal that the surface wave generated at the edge of the needle tip converges at the centre with damping due to the viscous effect, thus producing the projection. The micro bubbles are generated by the detachment of part of this projection. Therefore, the volume of the projection and the diameter of the daughter bubbles increase as the maximum volume of the mother bubble increases.

Both the shape of the mother bubble at maximum volume and d_b are relatively unaffected by changes in P_g when both d_{in} and the volume change in the mother bubble are large, as shown in Exp 6. This mode is often observed when the contact point between the mother bubble and the needle reaches the outer edge of the needle with increasing P_g (see also Exp. 7). This is the limitation of controlling d_b, and d_b remains relatively constant for higher P_g. However, the experimental results also show that producing daughter bubbles becomes increasingly difficult with increasing d_{out}. In the extreme case of d_{out}, therefore, no micro bubbles can be stably generated from a tiny hole on a plain surface. Therefore, d_{out} is also a controlling parameter in the stable generation of micro bubbles of uniform diameter.

Figure 11 shows the normalized daughter bubble diameter d^*_b $(=d_b/d_{in})$ as a function of normalized gas pressure inside the needle P^*_g for Exps 1 to 9. Note that for precise measurement of the d_b, instantaneous images were taken by using a CCD camera (KODAK, MEGAPLUS Camera ES1.0) with a resolution of 1008×1018 pixels and 1 pixel corresponds 0.45 μm. Because a strobe with an emission time of 180 ns (SUGAWARA, NP-1A) was used for the light source, the edges of the daughter bubbles were clearly detected. Because the bubble diameter also oscillates at a period due to the pressure change, the mean diameter of each bubble was calculated by averaging the measured diameters from several images, including images taken at the maximum volume of the mother bubble and at the detachment of the daughter bubble. Note that the deviation in the measured bubble diameters was less than 0.45 μm.

Figure 11 shows that d^*_b was relatively proportional to P^*_g when $0.04 < d^*_b < 0.08$ and that d_b can be controlled in this regime. Because the normalized d^*_b is within 0.04 to 0.08, under our experimental conditions, d^*_b increases as P^*_g increases. The

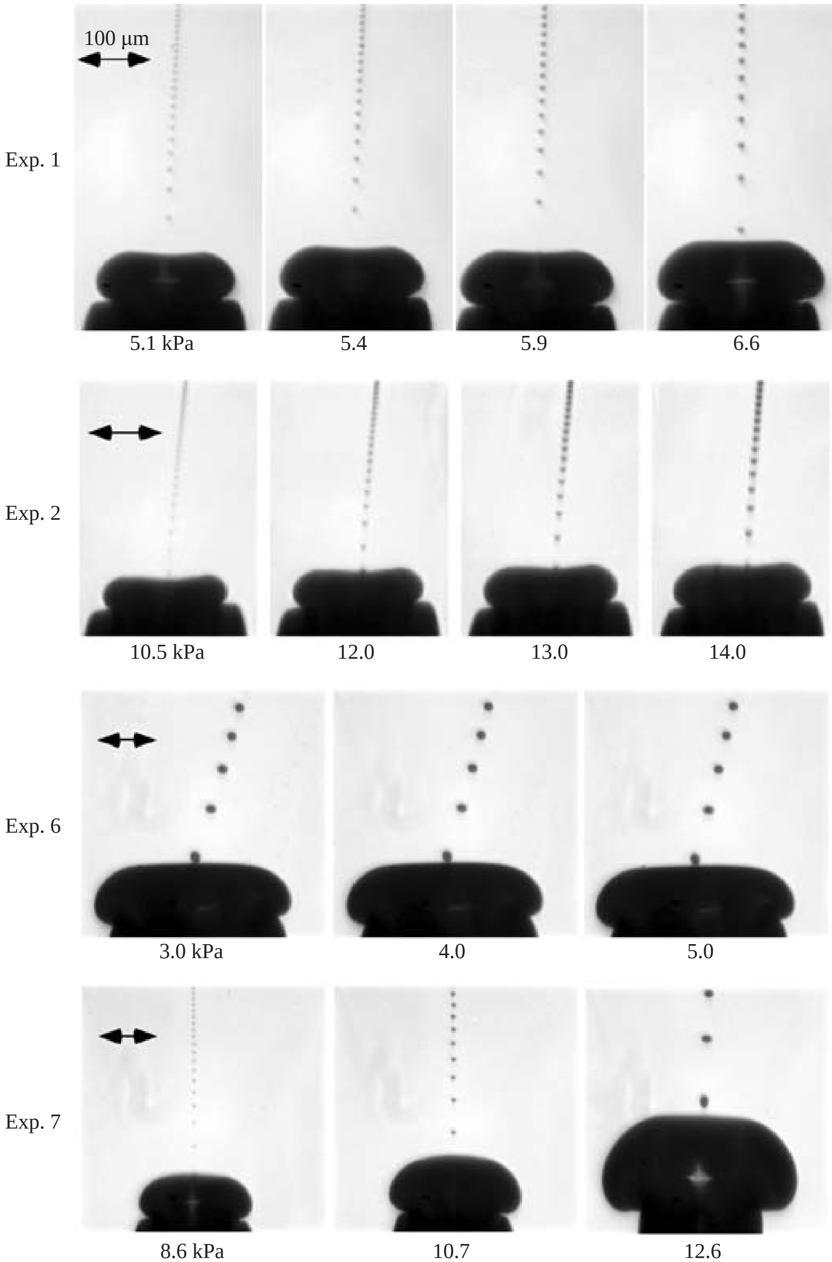

FIGURE 9. Instantaneous images of the evolution of produced bubbles at the maximum volume of the mother bubble as a function of increasing gas pressure P_g.

gradient $\partial d_b^* / \partial P_g^*$ is affected by *Wo*, *We* and $d_{out}^* (= d_{out}/d_{in})$. Comparing the results of Exps 1 and 7, the increase in *Wo* causes an increase in $\partial d_b^* / \partial P_g^*$. Comparison among the results of Exps 3, 7 and 8, all of which have similar *Wo* and d_{out}^*, shows that the increase in *We* also causes an increase in $\partial d_b^* / \partial P_g^*$. Inversely, the increase in d_{out}^* causes a decrease in $\partial d_b^* / \partial P_g^*$.

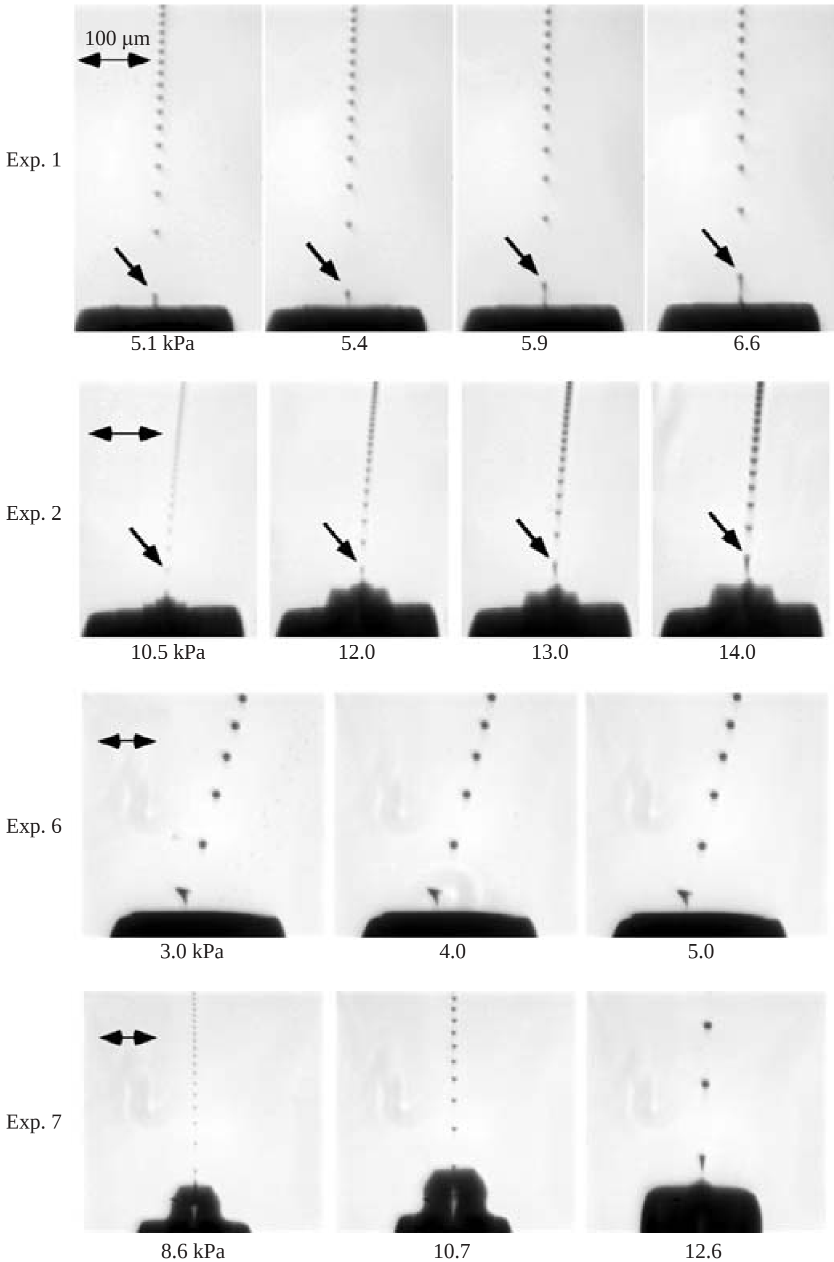

FIGURE 10. Instantaneous images of the evolution of produced bubbles immediately after the daughter bubble had detached from the mother bubble as a function of increasing gas pressure P_g.

The effects of parameters Wo, We and d^*_{out} on $\partial d^*_b/\partial P^*_g$ can be investigated based on dimensional analysis. Although P_{amp} also affects the conditions required for producing bubbles, its effect on d^*_b is small compared with the effect of other parameters (Wo, We and d^*_{out}) based on experimental observation and is therefore not considered in the following dimensional analysis.

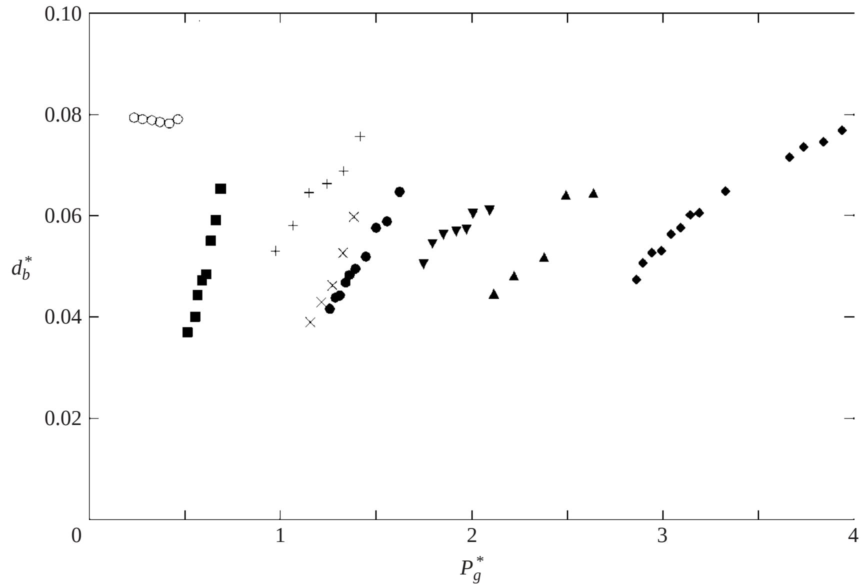

FIGURE 11. Gas pressure P_g^* versus normalized daughter bubble diameter d_b^*. ●, Exp. 1; ■; Exp. 2; ◆, Exp. 3; ×, Exp. 4; +, Exp. 5; ○, Exp. 6, ▲, Exp. 7; ▼ Exp. 8.

Exp.	Correlation equation
1	$d_b^* = 0.062P_g^* - 0.036$
2	$d_b^* = 0.163P_g^* - 0.049$
3	$d_b^* = 0.026P_g^* - 0.023$
4	$d_b^* = 0.090P_g^* - 0.066$
5	$d_b^* = 0.047P_g^* + 0.008$
7	$d_b^* = 0.042P_g^* - 0.045$
8	$d_b^* = 0.028P_g^* + 0.004$

TABLE 6. Values of $\partial d_b^*/\partial P_g^*$ obtained by linear regression.

Assuming that the dimensional parameters $d_{in}, d_{out}, f, P_g, \nu, \sigma$ and ρ affect d_b, the following five dimensionless parameters are obtained according to the π theorem.

$$\left[\frac{d_b}{d_{in}}\right]\left[\frac{P_g}{\rho f^2 d_{in}^2}\right]^{n_1}\left[\frac{\nu}{f d_{in}^2}\right]^{n_2}\left[\frac{\sigma}{\rho f^2 d_{in}^3}\right]^{n_3}\left[\frac{d_{out}}{d_{in}}\right]^{n_4} = [1]^0, \tag{4}$$

where the terms represent d_b^*, P_g^*, Wo^2,We and d_{out}^*, respectively. Assuming d_b^* is proportional to P_g^*, equation (4) becomes

$$\frac{\partial d_b^*}{\partial P_g^*} = a[Wo]^b[We]^c[d_{out}^*]^d. \tag{5}$$

Our experimental observation revealed that daughter bubbles are generated when P_g^* reaches a threshold value and that d_b is non-zero at $P_g^* = 0$. Therefore, we consider the effect of the controlling parameters Wo, We and d_{out} on the gradient $\partial d_b^*/\partial P_g^*$. The values of $\partial d_b^*/\partial P_g^*$ for data sets of Exps 1–5, 7 and 8 (Exp. 6 was not included because $\partial d_b^*/\partial P_g^* = 0$) were obtained by linear regression and are summarized in table 6. Based

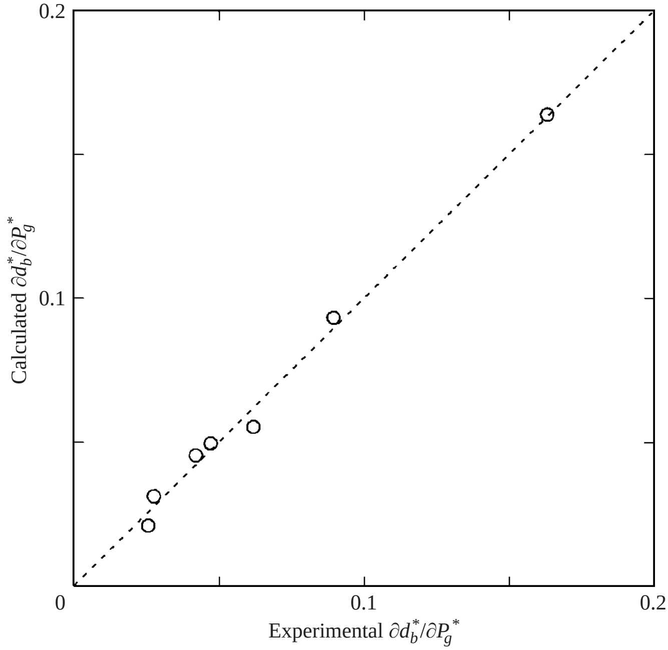

FIGURE 12. Experimental $\partial d_b^*/\partial P_g^*$ versus calculated $\partial d_b^*/\partial P_g^*$.

on these calculated values of $\partial d_b^*/\partial P_g^*$, the following values of a, b, c and d in equation (5) were determined by using a leasts-squares regression method:

$$\frac{\partial d_b^*}{\partial P_g^*} = 9.31 \times 10^{-3}[Wo]^{0.77}[We]^{0.60}[d_{out}^*]^{-1.07}. \tag{6}$$

Figure 12 shows the experimental values of $\partial d_b^*/\partial P_g^*$ versus the calculated values from equation (6). The calculated values agree relatively well with the experimental values. equation (6) shows that *Wo* and *We* similarly affect $\partial d_b^*/\partial P_g^*$. *We* is related to the Kelvin wavelength and *Wo* is related to the dissipation of the surface wave. This similar effects of *Wo* and *We* indicates that both *Wo* and *We* are important in controlling d_b.

By making the parameters in equation (6) dimensional, equation (6) becomes

$$\frac{\partial d_b}{\partial P_g} = 9.31 \times 10^{-3}\frac{d_{in}^{2.64}}{\rho^{0.40} f^{0.42} \nu^{0.39} \sigma^{0.60} d_{out}^{1.07}}. \tag{7}$$

Equation (7) indicates that the gradient $\partial d_b/\partial P_g$. becomes low with increasing f, ν, σ and d_{out} and that the controllability of d_b increases. d_b remains constant, however, when the mother bubble extends to the outer edge of the needle (see Exp. 6 in figures 9 and 10). Because micro bubbles are difficult to produce when d_{out} is too large, d_{out} should be selected with care. Equation (7) also shows that d_{in} affects d_b. The controllability of d_b increases with decreasing d_{in} because the gradient $\partial d_b/\partial P_g$ becomes low.

4. Summary

Consecutive images of the fragmentation of capillary waves in an ultrasonic field were obtained by using a high-speed video camera through a microscope at a frame rate of 500 000 frames per second. Results showed that micro bubbles of uniform diameter from 4 to 15 μm were generated at a constant periodic rate when a small amount of air was introduced (via a needle) into a highly viscous liquid whose kinematic viscosity was between 5 and 100 $mm^2 s^{-1}$ and whose surface tension was between 20 and 34 $mN m^{-1}$. When a mother bubble oscillated at the tip of the needle in the ultrasonic field, the surface wave generated near the inner edge of the needle propagated to the centre of the needle. A projection is formed on the gas–liquid interface of the mother bubble and micro bubbles are released from the tip of the projection. The experiments involving different gas viscosities showed that projections were rarely observed in the experiments involving hydrogen and carbon dioxide gases with viscosity lower than 15.0 μPa s. In contrast, projections were often observed in the experiments involving air and neon gas with viscosity of 18.6 and 31.7 μPa s, respectively, and the tip of the projection increased with increasing gas viscosity. However, the instability of the oscillation of the mother bubble increased in the case of neon gas because the induced projection was too large. In conclusion, stable micro bubble generation is critically affected by gas viscosity and is limited to around 20.0 μPa s. Because hydrodynamic effects (e.g. inertial, surface tension and viscous effects of liquid) are crucial for the stable generation of micro bubbles of uniform diameter, these effects were investigated as a function of Womersley number (Wo) and Weber number (We). The results revealed that micro bubbles of uniform diameter were stably generated when $8.16 < We < 300$ and $2 < Wo < 5$. When $Wo > 5$, the inertial effect dominated the viscous effect and many bubbles of various sizes were released from the gas–liquid interface of the mother bubble. When $Wo < 2$, the viscous effect dominated the inertial effect inversely and the interface was not distorted sufficiently to release the daughter bubble. When $We > 300$, the inertial effect dominated the surface tension effect and thus reduced the recovery force of the shape of the interface. Consequently, many bubbles of various sizes are released from the interface, as observed when $Wo > 5$. For small We, oscillation of the interface becomes stable without strong distortion, and owing to strong surface tension effect, no bubbles are generated. However, the minimum We for stable generation of micro bubbles of uniform diameter could not be determined because we could not obtain data for $We < 8.16$. The maximum variable region of P_{amp} and P_g was 5 kPa at the maximum and was critical for producing micro bubbles of uniform diameter. Micro bubbles of uniform diameter from 4 to 15 μm smaller than $0.34\,\lambda$ were produced. The diameter was not proportional to the capillary wavelength and was affected by parameters, including viscosity of the liquid and the inner and outer diameters of the needle, that have no relation to the capillary wavelength. When $8.16 < We < 300$ and $2 < Wo < 5$, the size of the daughter bubbles was relatively linearly controlled as a function of the gas pressure inside the needle. The gradient of this linear function can be expressed well as a function of Wo, We and the dimensionless outer diameter of the needle, and decreased either with increasing excitation frequency, kinematic viscosity, surface tension and outer diameter of the needle or with decreasing inner diameter of the needle.

This research is partially supported by the Japan Society for the Promotion of Science (Grant B-16360094).

REFERENCES

Brackbill, J. U., Kothe, D. B. & Zemach, C. 1992 A continuum method for modeling surface tension. *J. Comput. Phys.* **100**, 335–354.

Eggers, J. 2001 Air entrainment through free-surface cusps. *Phys. Rev. Lett.* **86**, 4290–4293.

Eisenmenger, W. 1959 Dynamic properties of the surface tension of water and aqueous solutions of surface active agents with standing capillary waves in the frequency range from 10kc/s to 1.5 Mc/s. *Acoustica* **9**, 327–340.

Hao, Y. & Prosperetti, A. 1999 The effect of viscosity on the spherical stability of oscillating gas bubbles. *Phys. Fluids* **11**, 1309–1317.

Kirpalani, D. M. & Toll, F. 2002 Revealing the physicochemical mechanism for ultrasonic separation of alcohol–water mixtures. *J. Chem. Phys.* **117**, 3874–3877.

Lang, R. J. 1962 Ultrasonic atomization of liquids. *J. Acoust. Soc. Am.* **34**, 6–8.

Prosperetti, A. 1977 Viscous effects on perturbed spheriacal flows. *Q. Appl. Maths* **34**, 339–352.

Rayleigh, Lord. 1945 *The Theory of Sound*, p. 344. Dover.

Staatman, A. G., Khayat, R. E., Haj-Qasem, E. & Steinman, D. A. 2002 On the hydrodynamic stability of pulsatile flow in a plane channel. *Phys. Fluids* **14**, 1938–1944.

Walmsley, A. D., Laird, W. R. E. & Williams, A. R. 1985 Gas bubble fragmentation in an ultrasonic field. *Ultrasonics* **23**, 170–172.